Transport Circulation Deduced from SAMS Trace Species Data

J. R. HOLTON AND WOO-KAP CHOI

Department of Atmospheric Sciences, University of Washington, Seattle, Washington

(Manuscript received 22 October 1987, in final form 27 January 1988)

ABSTRACT

Three years of zonally averaged N_2O and CH_4 data from the SAMS instrument on Nimbus 7 are utilized to investigate the annual and semiannual cycles in long-lived tracer mixing ratios. The annual and semiannual variations are shown to be approximately antisymmetric and symmetric about the equator, respectively. Using the first three components of the annual cycle to estimate the time tendency, the tracer continuity equation is solved diagnostically to obtain the effective transport velocity (i.e., the meridional circulation that can produce the observed seasonal variations in the tracer fields). The resulting circulation is qualitatively in agreement with the diabatic circulations computed by other workers. The present calculations, however, exhibit a stronger equinoctial subsidence in the equatorial upper stratosphere than deduced in other studies as required to produce a "double peak" tracer structure that has the amplitude and vertical extent that is observed.

1. Introduction

The mixing ratios of nitrous oxide (N_2O) and methane (CH_4) in the stratosphere were observed by the Stratospheric and Mesospheric Sounder (SAMS) instrument on the NIMBUS 7 satellite for more than 4 years. The accuracy of the SAMS data was discussed in detail by Jones and Pyle (1984); see also WMO (1986). Due to the poor signal-to-noise ratio of individual profiles, radiance data for the N_2O and CH_4 channels were zonally averaged before inversion. The zonally averaged mixing ratio fields have been archived for three complete years (1979–81). The data are available at 2.5° latitude intervals for the latitude range 50°S to 67.5°N, and 1.4 km vertical intervals for pressure levels from 15 to 0.7 mb for N_2O and 15 to 0.4 mb for CH_4. For each of these species, measurements are available for approximately 12 days per month.

Monthly mean cross sections for 1979 were published by Jones and Pyle (1984). Most of the major features of the 1979 monthly means also appear in the 1980 and 1981 data and are thus present in the three year average monthly means for 1979–81 (Jones 1984). For reference we have recomputed monthly mean composites for the years 1979–81. The resulting cross sections (Figs. 1 and 2) are nearly equal to those of Jones (1984).

The most significant feature of the mixing ratio fields shown in Figs. 1 and 2 is the strong vertical stratification. Since both of these tracers have sources at the ground and sinks in the middle and upper stratosphere, their mixing ratios decrease with height in the stratosphere. Furthermore, since the chemical lifetime of N_2O decreases with height more rapidly than does that of CH_4, the mixing ratio of N_2O decreases with height more rapidly than does that of CH_4. The vertical variation of N_2O can be approximated by an exponential decrease with height, while that of CH_4 can be approximated by a linear decrease with height.

For long-lived vertically stratified tracers the equilibrium slopes of constant mixing ratio surfaces in the meridional plane result from the competition between the slope steepening effects of advection by the diabatic meridional circulation, and the slope flattening effects of quasi-isentropic eddy transport and photochemical loss (Holton 1986; Mahlman et al. 1986). Thus, the general pattern shown in Figs. 1 and 2 of upward bulging mixing ratio surfaces in the equatorial region and downward slopes towards high latitudes is consistent with the well known stratospheric diabatic meridional circulation driven by eddies that produce departures from radiative equilibrium, which implies radiative heating and upward motion in low latitudes, poleward drift, and radiative cooling and subsidence in the extratropics.

Superimposed on this overall pattern there are, however, some substantial month to month variations in the meridional tracer distributions. Perhaps the most interesting such feature is the double peak structure, which can be observed from March to May for both tracers and in November with much weaker strength for N_2O only. The double peak structure, which has a minimum mixing ratio in the equatorial region surrounded by maxima in the subtropics, is nearly symmetric with respect to the equator. This symmetry sug-

Corresponding author address: Dr. James R. Holton, Dept. of Atmospheric Sciences, AK-40, University of Washington, Seattle, Washington 98195.

© 1988 American Meteorological Society

Unauthenticated | Downloaded 09/26/23 10:20 AM UTC

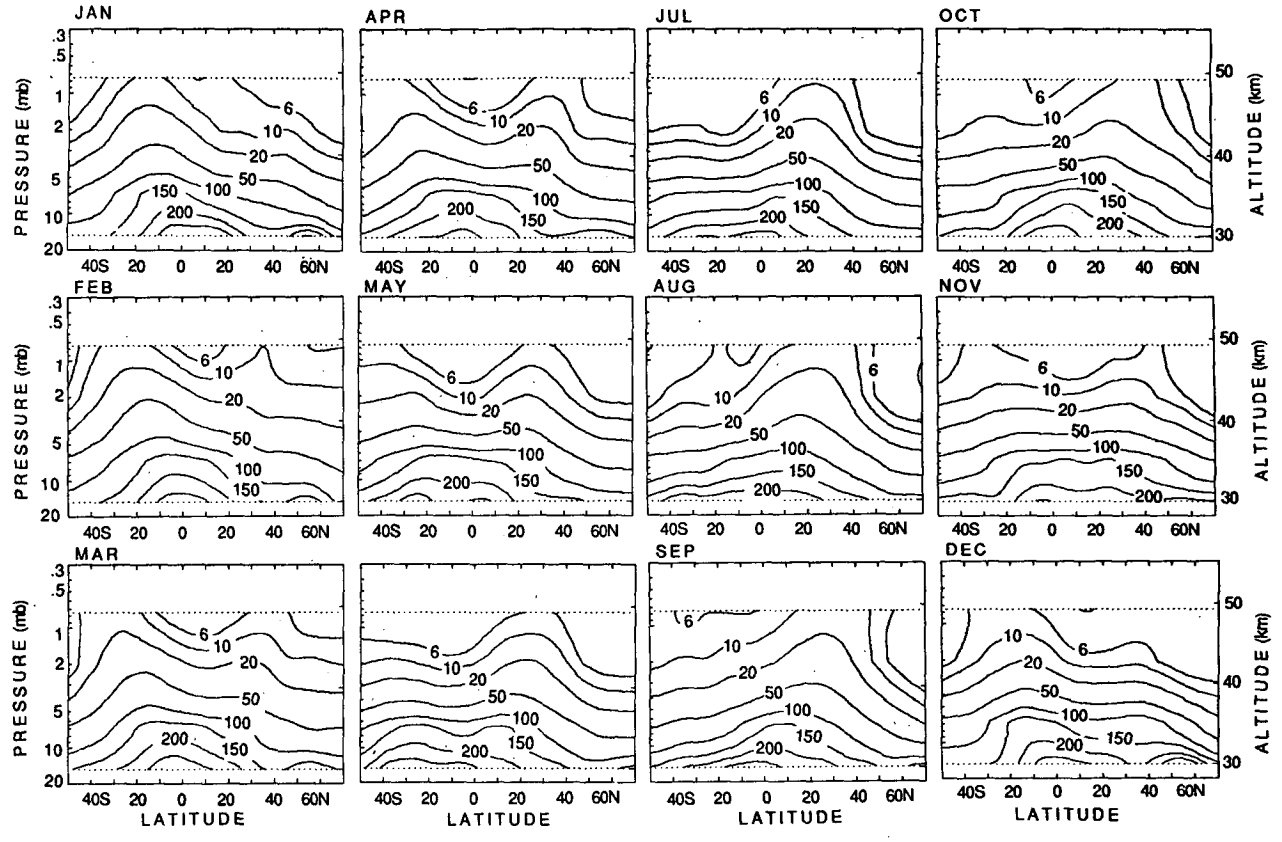

FIG. 1. Three year averaged monthly mean zonal mean cross sections of N_2O (ppbv) from January to December.

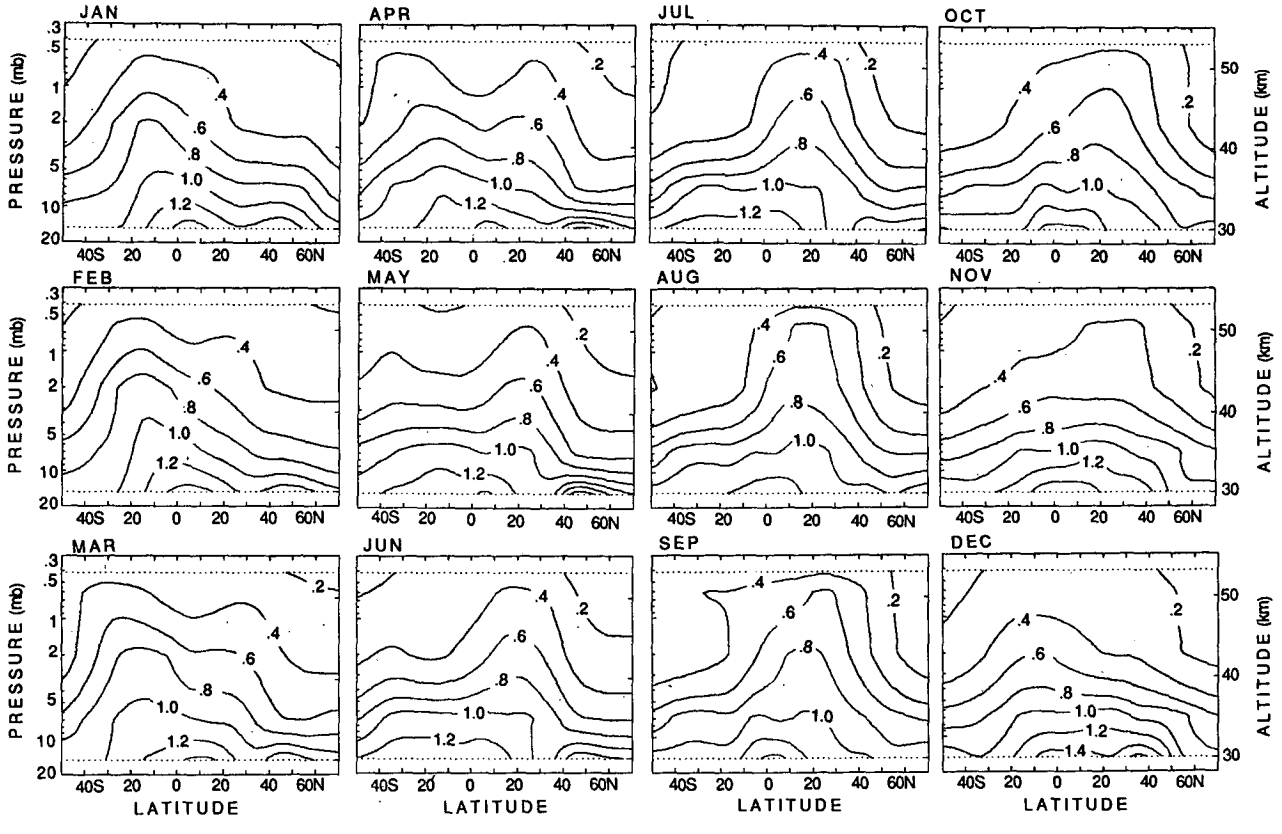

FIG. 2. As in Fig. 1 but of CH_4 (ppmv).

Unauthenticated | Downloaded 09/26/23 10:20 AM UTC

gests that it is associated with the semiannual oscillation of the equatorial zonal wind (SAO).

This conjecture was tested by Gray and Pyle (1986) using a transformed Eulerian mean (TEM) two-dimensional model. They included a semiannually varying westerly momentum source in the equatorial region, which forced an SAO in the zonal wind and temperature fields. (This parameterization was improved in Gray and Pyle 1987). The equatorial temperature maximum during the westerly phase of the simulated SAO at the equinoxes was maintained in the presence of radiative damping by a residual meridional circulation with subsidence near the equator and rising in the subtropics. Advection of the N_2O and CH_4 fields by this circulation produced double peaks in the equinoctial mixing ratio distributions, although the intensities of the double peaks were weaker than those observed.

In addition to the semiannual variability concentrated at low latitudes, the tracer cross sections of Figs. 1 and 2 clearly indicate an annual cycle, which tends to be antisymmetric about the equator with maxima occurring in the midlatitude region of the summer hemisphere.

The purpose of this paper is to document in some detail the nature of the annual and semiannual variations in the N_2O and CH_4 distributions, and to diagnose the structure of the meridional circulation that could account for the observed variations.

In section 2, time–latitude cross sections of the composition fields on a fixed pressure level are separated into components symmetric and antisymmetric about the equator. This separation clearly reveals the symmetric and antisymmetric character of the semiannual and annual variations, respectively. These are further documented through harmonic analysis of the monthly mean data.

In section 3, the first three components of the harmonic analysis (annual, semiannual and terannual cycles) are substituted into the tracer continuity equation and we attempt to determine the effective transport velocity (i.e., the meridional circulation that could produce the observed seasonal variations in the tracer distributions). The results are compared with the diabatic circulations deduced by other workers in section 4.

2. Data analysis

The mixing ratio data of N_2O and CH_4 comprise approximately 12 randomly scattered daily observations per month. Since the short time scale fluctuations of the mixing ratios are very large, the individual daily data are less meaningful than time averaged data, such as ten day means or monthly means. There are usually sufficient daily observations in each averaging period. In some periods, however, no data are available to compute the averages. In those cases, the adjacent values were used to deduce the averages by interpolation. In this study, ten day means and monthly means were composited over the three years available to enhance the statistical significance before doing any further computations.

Since the double peak structure mentioned in section 1 is restricted to only some months of the year and to the region above a certain level, its climatological importance is not obvious from the individual monthly mean cross sections. The climatological significance of the double peak becomes clear when monthly means for 3 years are averaged to produce the time mean cross sections shown in Figs. 3 and 4. As shown in Fig. 3, N_2O has a single peak up to the 5 mb level. Above that level the double peak is a significant feature, and the mixing ratio field tends to be symmetric about the equator, although the mixing ratios in the Northern Hemisphere are slightly larger than those in the Southern Hemisphere. The slope of the tracer mixing ratio isolines generally increases with height and latitude poleward of the equatorial double peak region; the steepest slope is found above the 2 mb level and to the north of 50°N. It is interesting that such a strong horizontal gradient of mixing ratio is retained in this region after time averaging, in view of rapid vertical decrease of mixing ratio elsewhere. In addition to the meridional circulation, latitudinally varying vertical diffusion might be one of the mechanisms which maintains this gradient. For CH_4, plotted in Fig. 4, most of the above discussion can be applied with only small changes. In the tropics of the Northern Hemisphere CH_4 has a strong maximum and the equatorial minimum is not distinct, although the double peak structure is present above the 2 mb level. The slopes of isolines also increase with height and latitude, and the isoline slopes are very steep in some regions. The time mean maps of both tracers show that peak values in the Northern Hemisphere are bigger than those in the Southern Hemisphere, although in the case of N_2O the differences are very small. This asymmetry between the hemispheres might be due to the strong planetary wave activity of

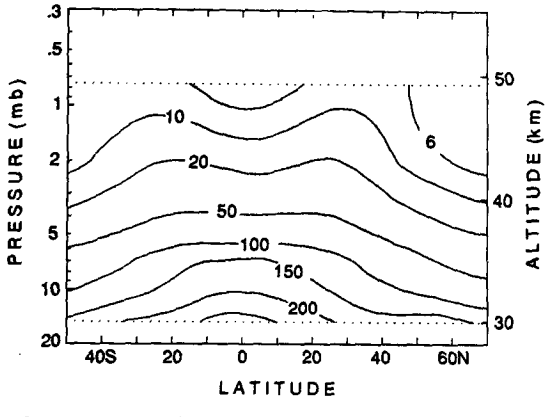

FIG. 3. Mean mixing ratio of N_2O (ppbv) for three years.

Unauthenticated | Downloaded 09/26/23 10:20 AM UTC

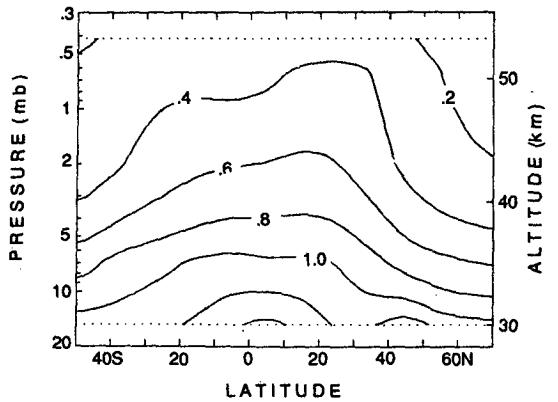

FIG. 4. As in Fig. 3 but of CH_4 (ppmv).

the Northern Hemisphere, for strong eddies enhance the diabatic mean meridional motion so that the mean tropical upwelling is likely to be stronger in the Northern Hemisphere.

The time mean cross sections of the two tracers are clearly similar in many aspects, and the month to month variations shown in Figs. 1 and 2 also have many similarities. To determine the relation between the variations of N_2O and CH_4 in an objective manner a correlation coefficient map is computed using the ten day averaged data for the 3 year time series. The result is shown in Fig. 5. In most regions, deviations of the mixing ratios of the two tracers from their 3 year means are positively correlated in time. The correlation coefficients are very large, especially in the tropical upper stratosphere where the double peak structure dominates the variability. Below the 5 mb level, where a single equatorial peak appears in the time mean map, the correlation coefficients are generally smaller than those in the upper stratosphere. The reason why the correlation coefficients are so small below the 5 mb level is not clear, but according to Jones and Pyle (1984) retrieval errors due to temperature uncertainties are much greater at 20 mb than above 7 mb. Thus, observational error may be to blame. At all pressure levels a minimum in the correlation pattern exists over the equatorial region and the correlations are usually stronger in the Southern Hemisphere than in the Northern Hemisphere. The fact that the highest correlations coincide with the double peak region implies that the temporal changes in the two tracers are affected by the same mechanism in that region despite the differences in their chemical destruction processes and time scales.

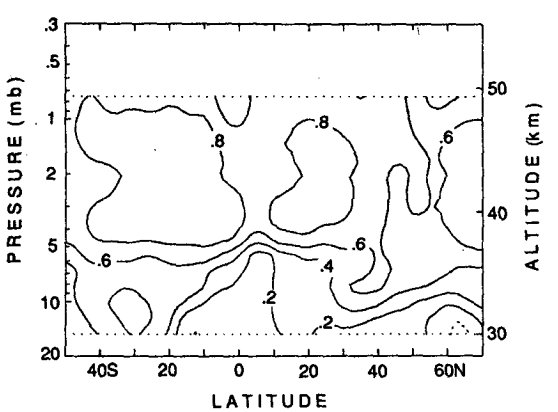

FIG. 5. Correlation coefficient cross section for 10-day means of the N_2O and CH_4 data for three years.

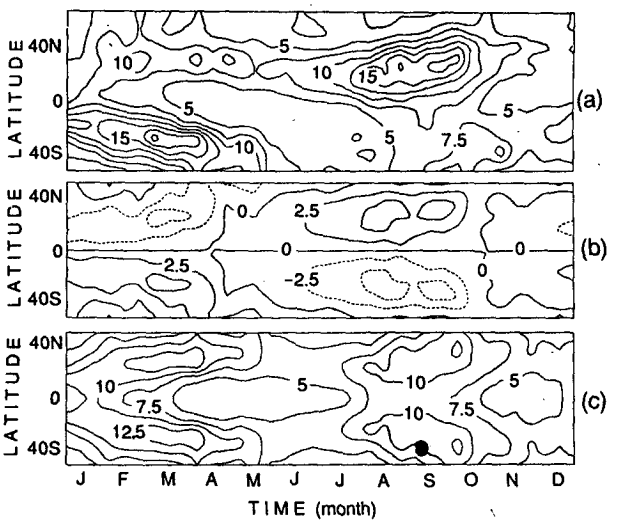

FIG. 6. (a) Three year averaged latitude cross section of N_2O (ppbv) on 1 mb level from January to December; (b) antisymmetric part of (a) with respect to the equator; (c) symmetric part of (a) with respect to the equator.

We now examine the double peak structure more closely by concentrating on the upper stratosphere. Figs. 6a and 7a are time–latitude cross sections at the 1 mb level made from 3 year averages of the ten day

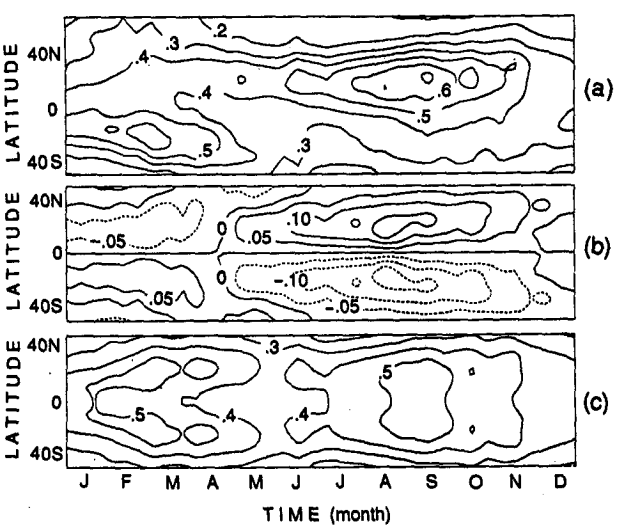

FIG. 7. As in Fig. 6 but of CH_4 (ppmv).

Unauthenticated | Downloaded 09/26/23 10:20 AM UTC

mean data. For both tracers, distinct maxima are shown in middle latitudes during summer and autumn in each hemisphere; these are evidently related to the annual oscillation. In addition to the two dominant maxima, each tracer also has a secondary maximum located in the Northern Hemisphere middle latitude for February to May. This represents the Northern Hemispheric branch of the double peak structure at the 1 mb level. There is no Southern Hemispheric counterpart 6 months later for CH_4 and only a very weak maximum for N_2O. These differences between the two secondary maxima may be regarded as evidence that the second SAO peak in each calendar year is weaker than the first, possibly reflecting the differences in the planetary waves in the two hemispheres. The time–latitude sections strongly suggest that the tracer variation is dominated by annual and semiannual components. The former is clearly present at extratropical latitudes, while in the equatorial region, the mixing ratio changes from large to small values twice as the month goes from January to December suggesting dominance of the semiannual oscillation.

The time–latitude fields are separated into components symmetric and antisymmetric about the equator in an attempt to better reveal the nature of the annual and the semiannual variations. The antisymmetric parts are shown in Figs. 6b and 7b and the symmetric parts in Figs. 6c and 7c. In the antisymmetric field, positive and negative values remain for about six months in each hemisphere and maxima appear in the midlatitude region of both hemispheres during summer. In Figs. 6b and 7b, CH_4 has a Northern Hemispheric summer maximum about double the strength of the Southern Hemisphere summer maximum, while N_2O has amplitudes in winter and summer that are quite comparable. In the symmetric field the mixing ratio values go through two oscillations per year at any latitude. Particularly at the equator, the first maximum appears in January and February and the second one in August and September while the first minimum appears in April and May and the second one in November. Hence, the interval between a maximum and an adjacent minimum is roughly 3 months. In middle latitudes, there are also maxima and minima and their amplitudes and periods show an almost sinusoidal oscillation. Thus, the antisymmetric and the symmetric fields approximately represent the annual and semiannual variations respectively.

To investigate the characteristics of the annual and semiannual variations of the mixing ratio distribution more completely, the monthly mean distribution is analyzed by Fourier series (i.e., using harmonic analysis). Figures 8 and 9 show the amplitude and the phase for the first harmonic and Figs. 10 and 11 for the second harmonic. In the phase map, a contour label means the month in which each component of mixing ratio has a maximum value. Hence, in the case of the semiannual component there is also a maximum at 6 months before or after the labeled month.

As shown in Figs. 8a and 9a the amplitude of the annual component for each tracer has a minimum in the equatorial region and maxima in the subtropics of both hemispheres. The maxima of N_2O are located at the 5 mb level, while the maxima of CH_4 are at the 2 mb level. The maximum amplitude in the Southern Hemisphere is bigger than its counterpart in the Northern Hemisphere in both cases. Figures 8b and 9b reveal that the Northern Hemispheric maximum appears in August in a broad region and the phase increases northwards. The phase changes rapidly by about 6 months around the equator (where the amplitude is very small). Thus, in the Southern Hemisphere the maximum values of the annual component also appear during summer. From the above analysis the annual component of the time series has a nearly symmetric amplitude distribution with a six month phase reversal over the equator.

The amplitude distributions of the semiannual component for N_2O and CH_4 shown in Figs. 10a and 11a, respectively, also have a symmetric structure with

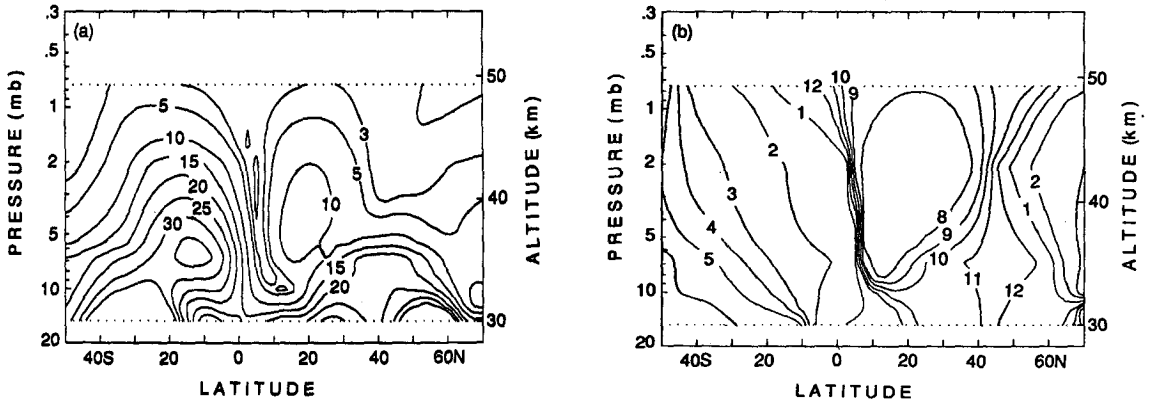

FIG. 8. (a) Amplitude of the annual harmonic of N_2O (ppbv); (b) phase of the annual harmonic. The contour labels indicate the months which have the maximum value.

Unauthenticated | Downloaded 09/26/23 10:20 AM UTC

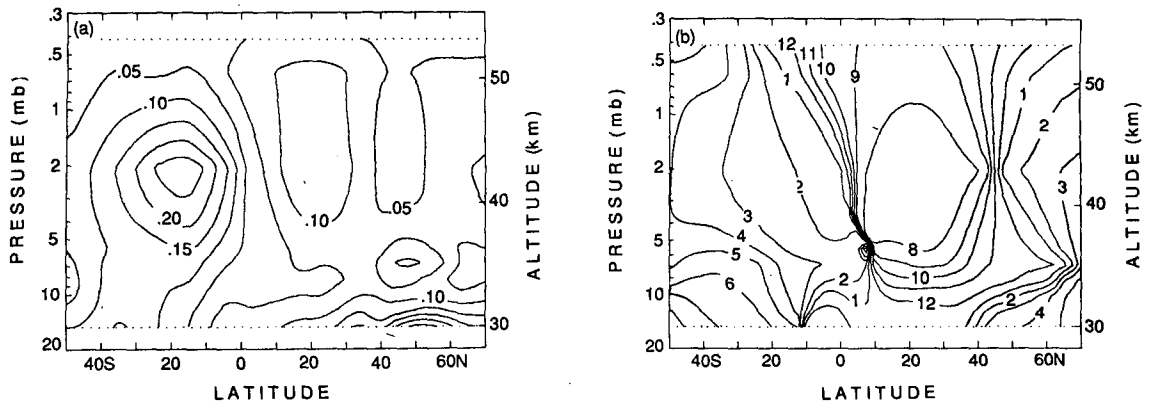

FIG. 9. As in Fig. 8 but of CH_4 (ppmv).

respect to the equator. The amplitudes are generally smaller than those of the annual harmonic so that the effect of the semiannual oscillation is less significant than the annual oscillation in most regions. In the upper stratosphere, however, the magnitudes of the annual and semiannual harmonics are comparable and hence their effects are also comparable. Over the equator the amplitude of the second harmonic is bigger than that of the first at all altitude levels, so that the dominant effect in that region comes from the semiannual oscillation rather than the annual oscillation.

In the equatorial region the phase maps Figs. 10b and 11b show distinct characteristics. In the case of N_2O, a downward phase propagation is seen clearly from April (October) to July (January). This propagation is similar to the downward propagation of the well known semiannual oscillation in the equatorial zonal wind (e.g., see Andrews et al. 1987 and references). The phase lines of CH_4 shown in Fig. 11b show less downward propagation than those of N_2O but the overall shapes are in good agreement with those of N_2O. The amplitude and the phase maps of the semiannual harmonic exhibit symmetric characteristics with respect to the equator.

The tendency for equatorial antisymmetry of the annual component, symmetry of the semiannual component and the time average suggests separating the fields into symmetric and antisymmetric portions; using only the antisymmetric part of the annual harmonic, the symmetric part of the semiannual harmonic and the time average. In fact, this process is employed to make a smoothed version of the Fourier components which are used to deduce the circulation pattern in section 3.

3. Transport circulation

One of the questions that naturally arises is what kind of circulation pattern can produce the observed mixing ratio field. We have only zonally averaged mixing ratio data available, and therefore if we have an appropriate two-dimensional formulation which includes the proper parameterization of the photochemical destruction and eddy diffusion, then we can solve the system to obtain the meridional circulation pattern.

There are various ways of formulating the two-dimensional transport problem. One popular scheme is based on the transformed Eulerian mean (TEM) equa-

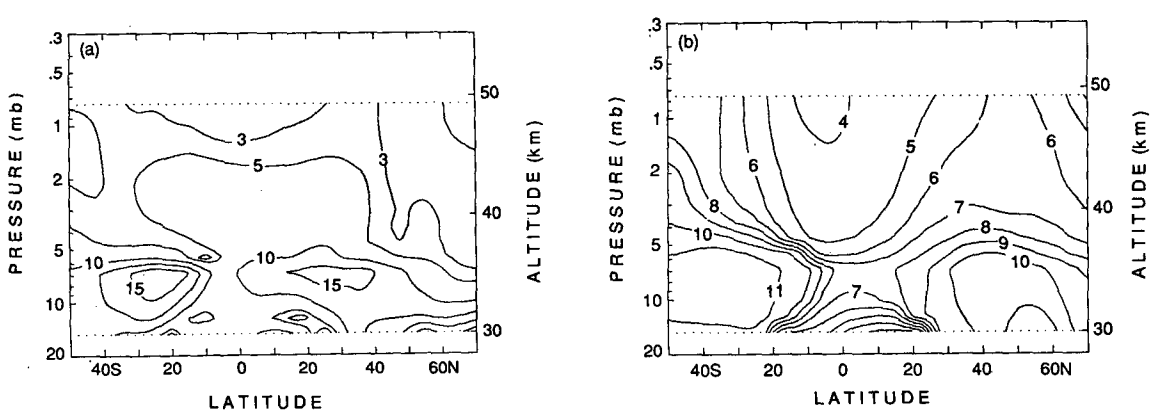

FIG. 10. (a) Amplitude of semiannual harmonic of N_2O (ppbv); (b) phase of semiannual harmonic. The contour labels indicate months which have the maximum value.

Unauthenticated | Downloaded 09/26/23 10:20 AM UTC

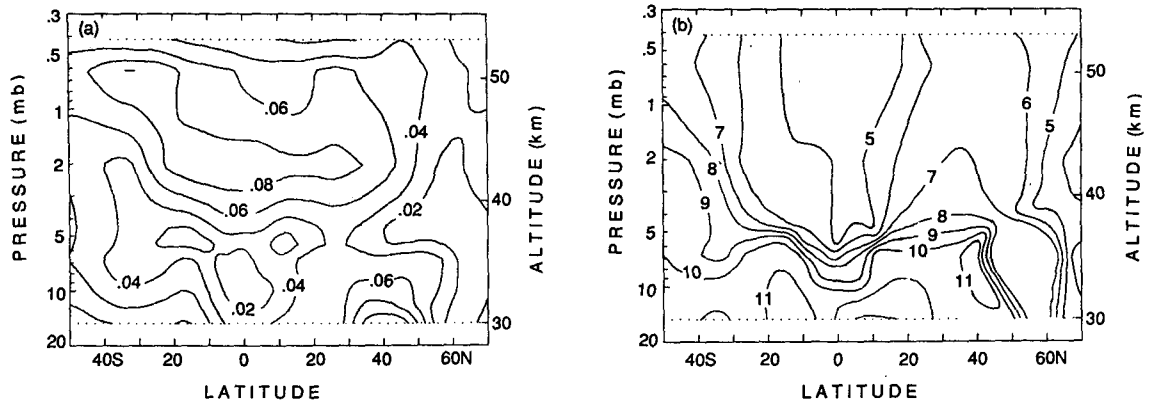

FIG. 11. (a) As in Fig. 10 but for CH_4 (ppmv).

tions. The TEM formalism does not, however, completely separate the advective and diffusive effects of transport. In this study, advective and diffusive effects are separated by defining the transport velocity as follows:

We start from the continuity equation for mixing ratio χ:

$$\frac{d\chi}{dt} = S \tag{1}$$

where S is the net source term.

Zonally averaging and manipulating gives (see Andrews et al. 1987 for detailed derivation)

$$\bar{\chi}_t + \bar{v}^\dagger \bar{\chi}_y + \bar{w}^\dagger \bar{\chi}_z = \bar{S} + \rho_0^{-1} \nabla \cdot (\rho_0 K \cdot \nabla \bar{\chi}) \tag{2}$$

in the spherical and log pressure coordinate system where an overbar means the zonal average, $\bar{v}^\dagger$ and $\bar{w}^\dagger$ are the components of the effective transport velocity (Plumb and Mahlman 1987), K is a symmetric diffusion tensor

$$K = \begin{pmatrix} K_{yy} & K_{yz} \\ K_{yz} & K_{zz} \end{pmatrix}$$

and

$$dy = a d\phi, \quad \rho_0 = \rho_s e^{-z/H}$$

where ϕ is the latitude, ρ_s is the global standard density and H is the scale height. The components of the effective transport velocity $\bar{v}^\dagger$ and $\bar{w}^\dagger$ are defined by

$$\bar{v}^\dagger \equiv \bar{v} + (2\rho_0)^{-1} [\rho_0 (\overline{v'\zeta'} - \overline{w'\eta'})]_z \tag{3a}$$

$$\bar{w}^\dagger \equiv \bar{w} - 2^{-1} (\overline{v'\zeta'} - \overline{w'\eta'})_y \tag{3b}$$

where η' and ζ' are parcel displacements such that

$$\left(\frac{\partial}{\partial t} + \bar{u} \frac{\partial}{\partial x} \right) (\eta', \zeta') \equiv (v', w') \tag{4}$$

and, like $(\bar{v}, \bar{w})$, also satisfy the continuity equation

$$(\cos\phi)^{-1} (\rho_0 \cos\phi \bar{v}^\dagger)_y + (\rho_0 \bar{w}^\dagger)_z = 0. \tag{5}$$

The effective transport velocity is generally different from the generalized Lagrangian mean velocity or the residual mean velocity $(\bar{v}^*, \bar{w}^*)$ (see Plumb and Mahlman 1987). We assume that the sink S is a linear photochemical loss

$$\bar{S} = -\alpha \bar{\chi} \tag{6}$$

and neglect the K_{yz}, K_{zz} components of the diffusion tensor K and retain only K_{yy} to the first approximation. So, (2) may be rewritten as

$$\bar{\chi}_t + \bar{v}^\dagger \bar{\chi}_y + \bar{w}^\dagger \bar{\chi}_z = -\alpha \bar{\chi} + K_{yy} \bar{\chi}_{yy}. \tag{7}$$

To solve (7), we define a mass flux streamfunction by

$$\psi_y = \rho_0 \bar{w}^\dagger \cos\phi, \quad \psi_z = -\rho_0 \bar{v}^\dagger \cos\phi \tag{8}$$

which satisfies the continuity equation automatically. Substituting relations (8) into (7) gives

$$\bar{\chi}_t - (\rho_0 \cos\phi)^{-1} \psi_z \bar{\chi}_y + (\rho_0 \cos\phi)^{-1} \psi_y \bar{\chi}_z = -\alpha \bar{\chi} + K_{yy} \bar{\chi}_{yy}. \tag{9}$$

In theory we could substitute the monthly mean mixing ratio distributions into (9), estimate the time derivative by finite differences and solve for $\psi(y, z, t)$. However, the zonally averaged monthly mean mixing ratio data from SAMS observations is highly variable and month to month fluctuations are very large even in the three year monthly mean composites. Thus, the resulting computed monthly mean transport fields are extremely noisy. We have found that much better results are obtained if we Fourier transform in the time domain (as in section 2) and retain only the time mean, annual, semiannual and terannual components of the variation. Additional smoothing is done by choosing only the antisymmetric portion of annual component and the symmetric portion of semiannual component and the time average. By the above procedure we eliminate the region from 50°N to 70°N but, for our purposes, this is not serious.

Unauthenticated | Downloaded 09/26/23 10:20 AM UTC

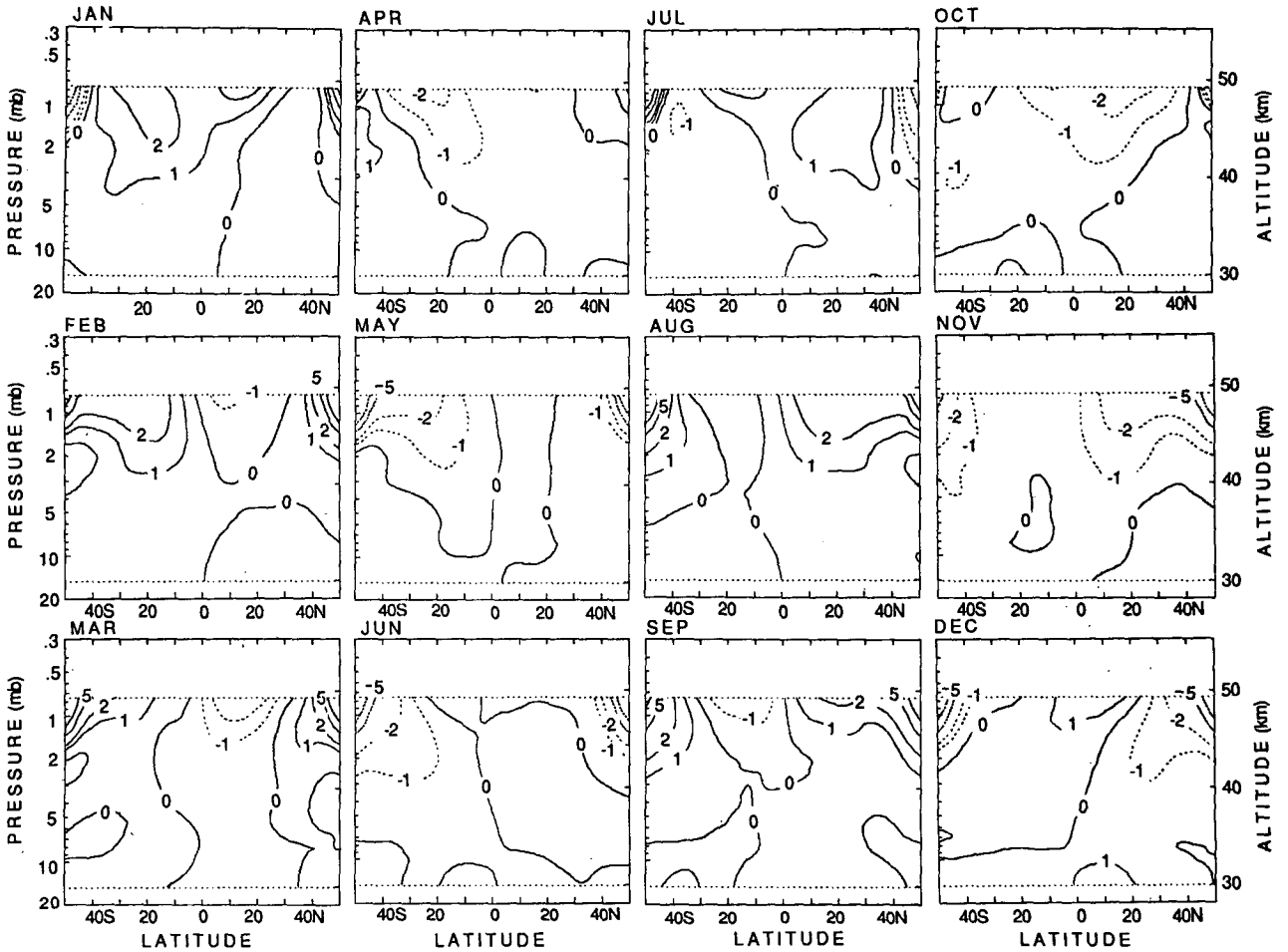

FIG. 12. Latitude–height cross sections of $\bar{w}^{\dagger}$ (mm s^{-1}) from January to December deduced by N_2O distribution. The contour labels are −10, −5, −2, −1, 0, 1, 2, 5 and 10.

To use the harmonics of the annual cycle we expand $\bar{\chi}$, ψ, $\bar{v}^{\dagger}$, $\bar{w}^{\dagger}$ as

$$\{\bar{\chi}, \psi, \bar{v}^{\dagger}, \bar{w}^{\dagger}\} = \sum_{n=-\infty}^{\infty} \{X_n, \Psi_n, V_n, W_n\} e^{in\omega t} \quad (10)$$

where $\omega = 2\pi/12$ months.

Substituting (10) into (9) we get, for the nth harmonic

$$(\Psi_n)_y + \gamma(\Psi_n)_z = \rho_0 \cos\phi[(\ln X_0)_z]^{-1} \times [(-in\omega - \alpha)X_n/X_0 + K_{yy}(X_n)_{yy}/X_0] \quad (11)$$

where $\gamma = -(\ln X_0)_y/(\ln X_0)_z$ is the slope of the isolines of X_0. Here, terms representing the interactions among the $n = 1, 2, 3$ harmonics are neglected. Equation (11) can be solved as an initial value problem in y to obtain Ψ_n; and V_n, W_n are obtained from Ψ_n by (8). Finally, finite series of V_n, W_n are used to construct the $\bar{v}^{\dagger}$, $\bar{w}^{\dagger}$ field. In this analysis we neglect time mean velocity components V_0 and W_0 and use harmonics $n = 1, 2, 3$ mentioned above.

The boundary conditions used for the numerical integration require careful consideration. The numerical integration for Ψ_1 was done in two steps. The values of Ψ_1 at the equator were obtained by integrating from 70°N to the equator using the original X_1 and setting Ψ_1 (70°N) = 0. The resulting Ψ_1 (0°) was then used as the boundary condition to deduce final Ψ_1 by integrating from the equator to 50° latitude using the smoothed (antisymmetric) X_1. The boundary conditions used for the numerical integrations for Ψ_2, Ψ_3 are Ψ_2 (0°) = 0 and Ψ_3 (70°N) = 0, respectively. At the upper and lower boundaries, linear extrapolation of Ψ_n is assumed.

The diffusion coefficient K_{yy} is given a constant value 10^5 m^2 s^{-1} consistent with the magnitudes used in the two-dimensional models of Solomon et al. (1986) and Ko et al. (1985). The chemical damping rate coefficients for the tracers are represented by height dependent functions based on values used in the Harvard 1-d model (Logan and Prather, personal communication; see Andrews et al. 1987, Fig. 9.2, for the profiles). No

Unauthenticated | Downloaded 09/26/23 10:20 AM UTC

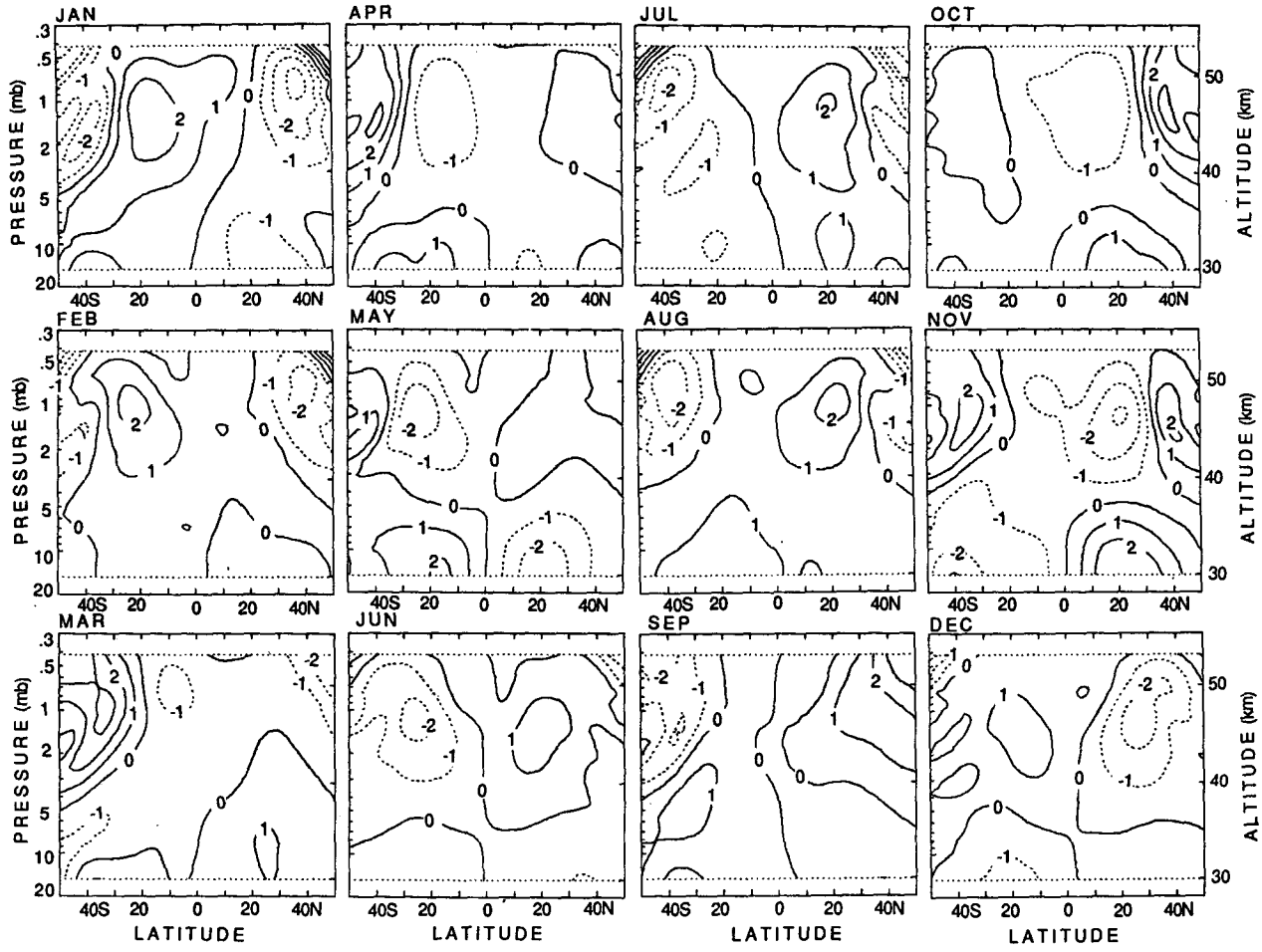

FIG. 13. As in Fig. 12 but by CH_4 distribution. The contour interval is 1 mm s^{-1}.

attempt was made to model the latitude and time variations of the damping rates since for these tracers the chemical term is small between 50°S and 50°N compared to the time tendency in Eq. (11).

The vertical component $\bar{w}^\dagger$ of effective transport velocity deduced by the numerical method discussed above is shown from January to December in Figs. 12 and 13. The main feature of the velocity distribution for both tracers is that a single cell circulation dominates near the solstices, with upward velocity in the summer hemisphere, downward velocity in the winter hemisphere and very small vertical velocity over the equator. This circulation pattern is qualitatively consistent with the diabatic circulation (Dunkerton 1978).

A different circulation pattern appears at the equinoxes, having a downward velocity in the equatorial region. This feature is best seen in March for N_2O. This downward velocity is consistent with the equatorial minimum mixing ratio at the time of the double peak. The velocity fields deduced from CH_4 look noisier than those for N_2O, but they still show the same pattern we observed in the case of N_2O. The noise in the CH_4 velocity field may be from small scale fluctuations of the CH_4 data that remain even after the space–time smoothing in our analysis.

In small regions near ±50° latitude in the upper stratosphere, very large vertical velocities appear for most months of the year. These values appear to be spurious. The reason for their presence might be as follows: in Fig. 3, there is a region where the slopes of the isolines are so steep that meridional diffusion must be very small compared to advection by the mean meridional circulation. In the calculation of $\bar{w}^\dagger$, the symmetric part of the time mean field (not shown) was used. The regions of steep slopes in the X_0 field correspond to the regions of unreasonably large velocities. In our computation of the velocity field the same value of the diffusion coefficient K_{yy} was used everywhere. If we assume that K_{yy} was overestimated for the region then the mean meridional circulation would also be overestimated to compensate for the diffusion. In the time mean map of CH_4, as shown in Fig. 4, the slopes are less steep than those of N_2O and hence the effect might be secondary. Another possible reason may be

Unauthenticated | Downloaded 09/26/23 10:20 AM UTC

the exclusion of the vertical diffusion in our computation which could have reduced the spurious velocities.

The time change of the vertical motion field is more easily seen in the time–latitude section at the 1 mb level shown in Figs. 14a and 15a. At the equator a downward velocity appears from March to May and also from September to November. Figures 14b and 15b show the antisymmetric field and Figs. 14c and 15c show the symmetric field, comparing these with Figs. 6 and 7 the relation between the upward (downward) and the high (low) mixing ratios can be seen. The vertical velocity field changes nearly simultaneously with the mixing ratio tendency, but the maximum mixing ratio lags the maximum in vertical motion.

4. Discussion and summary

In this study the zonal mean tracer continuity equation (2) was used diagnostically to determine the effective transport circulation. It is useful to compare this circulation with the residual meridional circulation of the transformed Eulerian mean system. The latter was determined diagnostically from the TEM version of the thermodynamic equation by Solomon et al. (1986), Hitchman and Leovy (1986) and Gille et al. (1987). In all of these papers observed zonal mean temperatures and ozone concentrations from the LIMS instrument on Nimbus 7 were used to compute the diabatic heating rates needed to determine the residual mean circulation.

Following Andrews et al. (1987) the TEM equation in the same coordinate system, as used in section 3, can be written as

$$\bar{\chi}_t + \bar{v}^*\bar{\chi}_y + \bar{w}^*\bar{\chi}_z = \bar{S} + \rho_0^{-1}\nabla \cdot M \qquad (12)$$

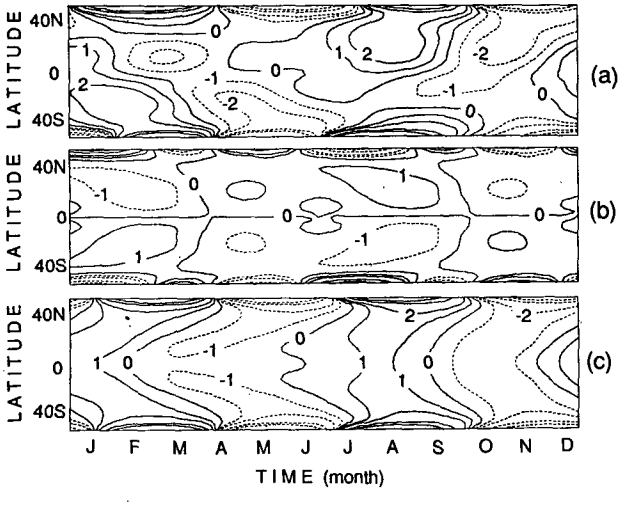

FIG. 14. (a) Time–latitude cross section of $\bar{w}^\dagger$ (mm s^{-1}) on 1 mb level deduced by N_2O distribution; (b) antisymmetric part of (a) with respect to the equator; (c) symmetric part of (a) with respect to the equator. The contour labels are −8, −5, −2, −1, 0, 1, 2, 5 and 8.

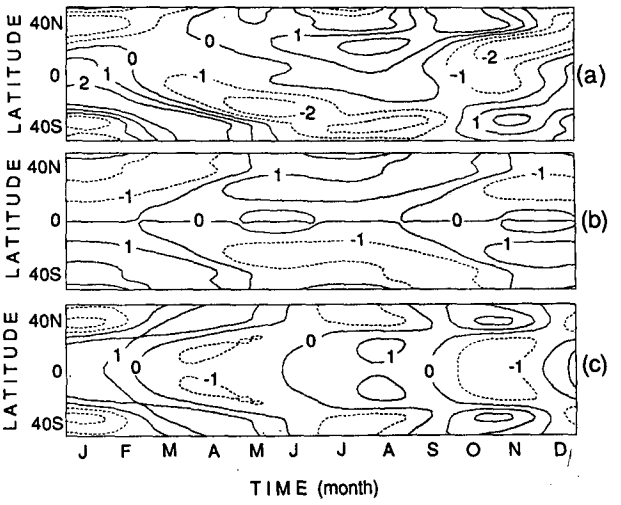

FIG. 15. As in Fig. 14 but deduced by CH_4 distribution. The contour interval is 1 mm s^{-1}.

where $\bar{v}^*$, $\bar{w}^*$ are residual mean velocities and

$$M = [-\rho_0(\overline{v'\chi'} - \overline{v'\theta'}\bar{\chi}_z/\bar{\theta}_z), \quad -\rho_0(\overline{w'\chi'} + \overline{v'\theta'}\bar{\chi}_z/\bar{\theta}_z)]. \qquad (13)$$

The residual mean velocity is, in general, different from the effective transport velocity (Plumb and Mahlman 1987). Unlike the effective transport velocity form of the continuity equation (2), the TEM form does not completely separate advective and diffusive effects of the eddies since M generally makes a contribution to the total advective transport. However, the difference between the two velocities is usually small in the stratosphere, except in the extratropical region in winter. If the waves are linear, steady and adiabatic then even in the presence of mechanical damping

$$\bar{v}^\dagger = \bar{v}^*, \quad \bar{w}^\dagger = \bar{w}^*, \qquad (14)$$

(for proof see Andrews et al. 1987).

The $\bar{w}^*$ fields computed by Solomon et al. (1986), Hitchman and Leovy (1986) and Gille et al. (1987) show that the effective transport velocity and the residual mean velocity are qualitatively similar. In particular, at the solstices the same pattern, i.e., upward velocity in the summer hemisphere and downward velocity in the winter hemisphere dominate although there are some differences in the amplitudes of the vertical velocity. Also, in the figures of Solomon et al. (1986), Hitchman and Leovy (1986) and Gille et al. (1987), subsidence begins to appear at high altitudes over the equator in December and then propagates downward until February. This is similar to our results, which show a downward directed effective transport velocity in the equatorial upper stratosphere in February (Figs. 12 and 13). Differences, however, arise in springtime. In the results of Solomon et al. (1986), upward diabatic motion occupies the equatorial region

Unauthenticated | Downloaded 09/26/23 10:20 AM UTC

in contrast to the downward effective transport velocity in our results for the same period. In the study of Hitchman and Leovy (1986) the $\bar{w}^*$ field shown for spring is weaker than that of this study. Gille et al. (1987) show an equatorial subsidence in the 30–40 km altitude range during March and April, but it is also very weak. Our results show that the typical maximum stratopause descent velocities for spring are $1 \sim 2$ mm s^{-1} and these are twice as large as the diabatic vertical velocities deduced from LIMS. Direct comparison might not be appropriate since the data sources are different. Particularly in the "V5" LIMS version used by Solomon et al. (1986), the amplitude of the SAO is less pronounced than in the "V4" version used by Hitchman and Leovy (1986), as they pointed out.

In the above discussion we compared the effective transport velocity determined by the 3 year observations of tracer distribution with the residual mean velocity estimated from the net heating rate. They are qualitatively similar in that small values of the mixing ratio occur with downward transport and large values with upward transport.

The double peak structure with the equatorial minima is related to this seasonal variation of the velocity field and is clearly related to the semiannual oscillation. Finally, the difference between the effective transport velocity field and residual mean velocity field and the physical processes controlling the tracer distribution in the region with the extremely steep slope need more investigation.

Acknowledgments. The authors are grateful to Dr. M. Hitchman for useful suggestions on an early draft of this manuscript. This work was supported by the National Aeronautics and Space Administration under NASA Grant NAGW-662, and the National Meteorology Program of the National Science Foundation, NSF Grant ATM-8314111.

REFERENCES

Andrews, D. G., J. R. Holton and C. B. Leovy, 1987: *Middle Atmosphere Dynamics,* Academic Press, 489 pp.

Dunkerton, T., 1978: On the mean meridional mass motions of the stratosphere and mesosphere. *J. Atmos. Sci.,* **35,** 2325–2333.

Gille, J. C., L. V. Lyjak and A. K. Smith, 1987: The global residual mean circulation in the middle atmosphere for the northern winter period. *J. Atmos. Sci.,* **44,** 1437–1452.

Gray, L. G., and J. A. Pyle, 1986: The semiannual oscillation and equatorial tracer distributions. *Quart. J. Roy. Meteor. Soc.,* **116,** 387–407.

——, and ——, 1987: Two dimensional model studies of equatorial dynamics and tracer distributions. *Quart. J. Roy. Meteor. Soc.*

Hitchman, M. H., and C. B. Leovy, 1986: Evolution of the zonal mean state in the equatorial middle atmosphere during October 1978–May 1979. *J. Atmos. Sci.,* **43,** 3159–3176.

Holton, J. R., 1986: Meridional distribution of stratospheric trace constituents. *J. Atmos. Sci.,* **43,** 1238–1242.

Jones, R. L., 1984: Satellite measurements of atmospheric composition: Three years' observations of CH_4 and N_2O. *Adv. Space Res.,* **4,** 121–130.

——, and J. A. Pyle, 1984: Observations of CH_4 and N_2O by the NIMBUS 7 SAMS: A comparison with in-situ data and two-dimensional numerical model calculations. *J. Geophys. Res.,* **89,** 5263–5279.

Ko, M. K. W., K. K. Tung, D. K. Weisenstein and N. D. Sze, 1985: A zonal mean model of stratospheric tracer transport in isentropic coordinates: Numerical simulations for nitrous oxide and nitric acid. *J. Geophys. Res.,* **90,** 2313–2329.

Mahlman, J. D., H. Levy II and W. J. Moxim, 1986: Three-dimensional simulations of stratospheric N_2O: Predictions for other trace constituents. *J. Geophys. Res.,* **91,** 2687–2707.

Plumb, R. A., and J. D. Mahlman, 1987: Zonally averaged transport characteristics of the GFDL general circulation/transport model. *J. Atmos. Sci.,* **44,** 298–327.

Solomon, S., J. T. Kiehl, R. R. Garcia and W. Grose, 1986: Tracer transport by the diabatic circulation deduced from satellite observations. *J. Atmos. Sci.,* **43,** 1603–1617.

WMO, 1986: *Atmospheric Ozone 1985,* World Meteor. Organ., Geneva.

Unauthenticated | Downloaded 09/26/23 10:20 AM UTC